Aggregation-Induced Emission in the Crystals of 9,10-Distyrylanthracene Derivatives: The Essential Role of Restricted Intramolecular Torsion

Jiating He, Bin Xu, Feipeng Chen, Haijian Xia, Kunpeng Li, Ling Ye, and Wenjing Tian*

State Key Laboratory of Supramolecular Structure and Materials, Jilin University, Changchun, 130012, P. R. China

Received: January 8, 2009; Revised Manuscript Received: April 28, 2009

We have studied the crystal structures and photophysical properties of four 9,10-distyrylanthracene (DSA) derivatives. Their crystal structures exhibit nonplanar conformations due to the supramolecular interactions resulting in rigid molecules and relative tight stacking. The four DSA derivatives possess a typical aggregation-induced emission (AIE) property, i.e., they exhibit faint emission in their solutions but intense emission in their crystals as a result of the dominant nonradiative decay by free intramolecular torsion in the solution and the restricted torsional motion by supramolecular interaction in the crystal. The investigation of the relationship between the crystal structures and AIE properties of the four DSA derivatives indicates that DSA moiety is the key factor of AIE property because of the restricted intramolecular torsion between the 9,10-anthrylene core and the vinylene moiety.

Introduction

π-conjugated organic molecules have attracted considerable interest in both academic research and industrial applications due to their increasing potentials as active components for optical and electronic devices such as organic light-emitting diodes (OLEDs).[1−4] However, aggregation which exists widely in π-conjugated organic molecules decreases the photoluminescence (PL) quantum yield dramatically when they are fabricated into solid thin films.[5−7]

Recently, molecules with AIE properties have drawn more and more attention, because of their enhanced emission in the aggregates. Tang et al. and Park et al. have reported several molecules with AIE properties, such as 1,1-substituted 2,3,4,5-tetraphenylsilole derivatives[8] and styrylbenzene derivatives.[9] AIE-active molecules are normally significantly emissive in their crystalline forms which possess higher carrier mobility to afford high current injection compared to amorphous forms.[10] Thus, they are potential candidates as the active layer in OLEDs and electrically pumped lasers.[11] So it is significantly important to develop crystals with AIE properties.

Up to now, few AIE-active molecules with anthrylene core have been reported. Prasad et al. have reported 9,10-bis[4′-(4″-aminostyryl)styryl]anthracene (BDSA-Bz), which exhibited weak emission in a true solution, but enhanced fluorescence in bulk-solid or nanoaggregated dispersions.[12] By semiempirical molecular orbital calculations, they speculated that the partially distorted geometry in the aggregated state is the reason for the aggregation-enhanced emission of BDSA-Bz. Fabian et al. had reported the synthesis of several DSA derivatives,[13] but they only found that these molecules showed weak fluorescence in their solutions. As far as we know, there is no report on the crystal structure of AIE-active molecules with anthrylene core.

Here, we have designed and synthesized a series of AIE-active DSA derivatives DSA, BMOSA, B-4-BOSA, and B-2-BOSA (their molecular structures are shown in Chart 1) and have grown their single crystals. Comparing the crystal structures of these AIE-active molecules, we find that all the chromophores have a nonplanar conformation in their crystalline states, which is probably attributed to the supramolecular interactions resulting in relatively tight packing and rigid molecules. Further study on the intrinsic luminescence properties of these nonplanar conjugated molecules demonstrates that the restricted intramolecular torsion between the 9,10-anthrylene core and the vinylene moieties plays an important role in AIE properties of these DSA derivatives.

Experimental Section

General. All reagents and starting materials are commercially available and were used as received. 9,10-Dibromoanthracene was purchased from Acros and used without further purification. DMAc was purified by fractional distillation before use as solvent. As shown in Scheme 1, 1-methoxy-4-vinylbenzene (**2**), 1-butoxy-4-vinylbenzene (**3**), and 1-butoxy-2-vinylbenzene (**4**) were prepared according to literature procedures.[14] The ^{1}H NMR spectra and the ^{13}C NMR spectra were recorded at 298 K onan AVANCZ 500 spectrometer and Varian Mercury-300 NMR, respectively, with teramethylsilame (TMS) as the standard. The compounds were characterized by a Flash EA 1112, CHNS-O elemental analysis instrument. The time-of-flight mass spectra were recorded with a Kratos MALDI-TOF mass system.

UV−vis absorption spectra were recorded on a UV-3100 spectrophotometer. Fluorescence measurements were carried out with RF-5301PC. Crystalline state PL efficiencies were measured with an integrating sphere (C-701, Labsphere Inc.), with a 325-nm Xe light as the excitation source, and the laser was introduced into the sphere through the optical fiber.

Single crystals of all the compounds were prepared by vaporizing mixed solvents of chloroform and ethanol (2:1) slowly at room temperature under rigorous exclusion of light. The diffraction experiments were carried out on a Rigaku R-AXIS RAPID diffractometer equipped with Mo Kα and Control Software, using the RAPID AUTO at 293($\pm$2) K. Empirical absorption corrections were applied automatically. The structures were solved with direct methods and refined with

* Corresponding author. Email: wjtian@jlu.edu.cn Fax: +86 431 851693421 (Prof. W. J. Tian).

10.1021/jp900205k CCC: $40.75
Published on Web 05/08/2009

CHART 1: Chemical Structures of 9,10-Distyrylanthracene Derivatives

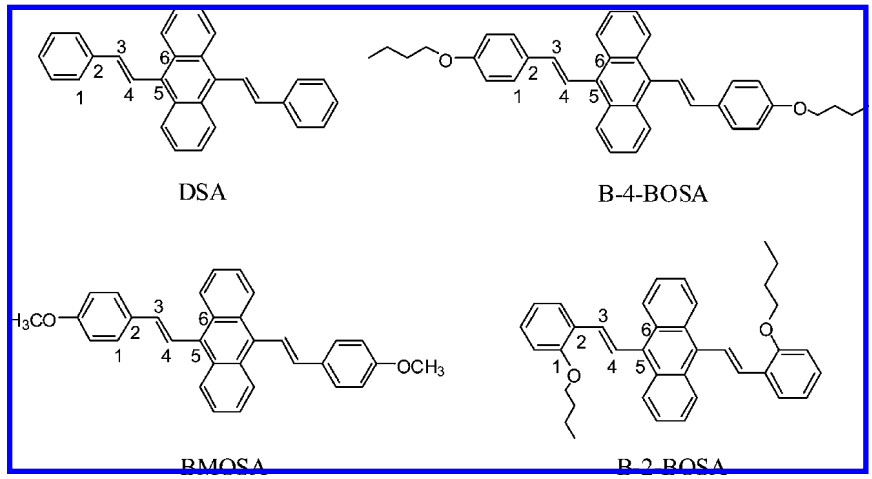

SCHEME 1: Preparation of 9,10-Distyrylanthracene Derivatives (1a−4a)

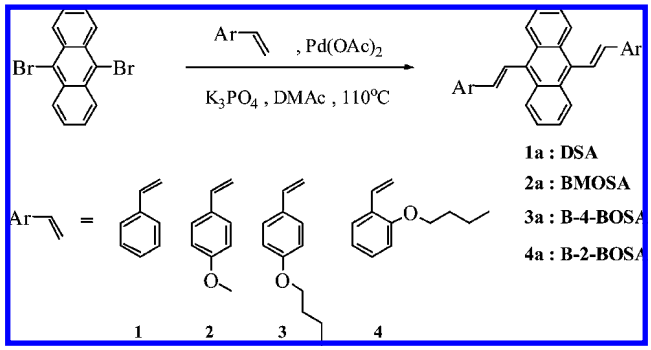

a full-matrix least-squares technique, using the SHELXS v. 5.1 programs, respectively. The space groups were determined from the systematic absences and their correctness was confined by successful solution and refinement of structures. Anisotropic thermal parameters were refined for all the non-hydrogen atoms. The hydrogen atoms were added in idealized position and refined with isotropic displacement. Crystallographic data for the structures reported in this paper are given in CIF files (Supporting Information).

Synthesis of 9,10-Distyrylanthracene (DSA, 1a). A round-bottomed flask (25 mL) was oven-dried and cooled under N_2 atmosphere. Styrene (0.042 g, 0.4 mmol), 9,10-dibromoanthracene (0.24 g, 0.72 mmol), K_3PO_4 (0.21 g, 1 mmol), and $Pd(OAc)_2$ were dissolved in dry DMAc (10 mL). The reaction mixture was heated to 110 °C in an oil bath and stirred for 24 h at this temperature. After being cooled to room temperature, the reaction mixture was poured into water and extracted with CH_2Cl_2 (3 × 40 mL). The combined organic extracts were washed with brine, dried (Mg_2SO_4), and concentrated to dryness under vacuum. The crude product was purified by flash column chromatography (petroleum ether/CH_2Cl_2 = 4:1) to give 0.113 g of product DSA as a yellow solid (41% yield). ^{1}H NMR (500 MHz, $CDCl_3$, TMS, ppm) δ 6.95 (d, J = 16.5 Hz, 2H, CH═CH), 7.37 (t, J = 7.5 Hz, 2H, Ar), 7.46−7.49 (m, 8H, Ar), 7.70 (d, J = 7.5 Hz, 4H, Ar), 7.94 (d, J = 16.5 Hz, 2H, CH═CH), 8.39−8.41 (m, 4H, Ar); ^{13}C NMR (75 MHz, $CDCl_3$, TMS, ppm) δ 137.46, 137.28, 132.68, 129.56, 128.84, 128.03, 126.60, 126.46, 125.24, 125.16; MALDI/TOF MS calcd for $C_{30}H_{22}$ 382.2, found 382.6. Anal. Calcd for $C_{30}H_{22}$: C, 94.20; H, 5.80. Found: C, 94.08; H, 5.89.

Synthesis of 9,10-Bis(4-methoxystyryl)anthracene (BMOSA, 2a). BMOSA was prepared according to the same procedure as that of DSA from 1-methoxy-4-vinylbenzene (0.32 g, 2.4 mmol), 9,10-dibromoanthracene (0.34 g, 1 mmol), K_3PO_4 (0.64 g, 3 mmol), and $Pd(OAc)_2$. Column chromatography (petroleum ether/CH_2Cl_2 = 4:1) gave 0.29 g of a yellow solid (65% yield). ^{1}H NMR (500 MHz, $CDCl_3$, TMS, ppm) δ 3.89 (s, 6H, OCH_3), 6.88 (d, J = 16.5 Hz, 2H, CH═CH), 7.00 (d, J = 8.5 Hz, 4H, Ar), 7.45−7.47 (m, 4H, Ar), 7.63 (d, J = 8.5 Hz, 4H, Ar), 7.79 (d, J = 16.5 Hz, 2H, CH═CH), 8.39−8.41 (m, 4H, Ar); ^{13}C NMR (75 MHz, $CDCl_3$, TMS, ppm) δ 159.73, 136.90, 132.83, 130.35, 129.73, 127.83, 126.55, 125.10, 123.05, 114.35, 55.45; MALDI/TOF MS calcd for $C_{32}H_{26}O_2$ 442.5, Found 443.4. Anal. Calcd for $C_{32}H_{26}O_2$: C, 86.85; H, 5.92. Found: C, 86.71; H, 6.01.

Synthesis of 9,10-Bis(4-butoxystyryl)anthracene (B-4-BOSA, 3a). B-4-BOSA was prepared according to the same procedure as that of DSA from 1-butoxy-4-vinylbenzene (0.21 g, 1.2 mmol), 9,10-dibromoanthracene (0.17 g, 0.5 mmol), K_3PO_4 (0.32 g, 1.5 mmol), and $Pd(OAc)_2$. Column chromatography (petroleum ether/CH_2Cl_2 = 4:1) gave 0.19 g of a yellow solid (72% yield). ^{1}H NMR (500 MHz, $CDCl_3$, TMS, ppm) δ 1.00 (t, J = 7.5 Hz, 6H, CH_3), 1.50−1.57 (m, 4H, CH_2CH_3), 1.79−1.84 (m, 4H, $CH_2C_2H_5$), 4.03 (t, J = 6.5 Hz, 4H, OCH_2), 6.87 (d, J = 16.5 Hz, 2H, CH═CH), 6.98 (d, J = 8.5 Hz, 4H, Ar), 7.44−7.46 (m, 4H, Ar), 7.60 (d, J = 8.5 Hz, 4H, Ar), 7.77 (d, J = 16.5 Hz, 2H, CH═CH), 8.38−8.40 (m, 4H, Ar); ^{13}C NMR (75 MHz, $CDCl_3$, TMS, ppm) δ 159.19, 136.91, 132.80, 130.01, 129.64, 127.77, 126.54, 125.07, 122.75, 114.84, 67.87, 31.35, 19.28, 13.89; MALDI/TOF MS calcd for $C_{38}H_{38}O_2$ 526.3, found 526.6. Anal. Calcd for $C_{38}H_{38}O_2$: C, 86.65; H, 7.27. Found: C, 86.56; H, 7.30.

Synthesis of 9,10-Bis(2-butoxystyryl)anthracene (B-2-BOSA, 4a). B-2-BOSA was prepared according to the same procedure as that of DSA from 1-butoxy-2-vinylbenzene (0.21 g, 1.2 mmol), 9,10-dibromoanthracene (0.17 g, 0.5 mmol), K_3PO_4 (0.32 g, 1.5 mmol), and $Pd(OAc)_2$. Column chromatography (petroleum ether/CH_2Cl_2 = 4:1) gave 0.18 g of a yellow solid (70% yield). ^{1}H NMR (500 MHz, $CDCl_3$, TMS, ppm) δ 0.92 (t, J = 7.5 Hz, 6H, CH_3), 1.46−1.54 (m, 4H, CH_2CH_3), 1.76−1.81 (m, 4H, $CH_2C_2H_5$), 4.06 (t, J = 6.5 Hz, 4H, OCH_2), 6.98 (d, J = 8.0 Hz, 2H, Ar), 7.07 (t, J = 7.5 Hz, 2H, Ar), 7.29 (d, J = 17.0 Hz, 2H, CH═CH), 7.32 (t, J = 8.0 Hz, 2H, Ar), 7.46−7.48 (m, 4H, Ar), 7.82 (d, J = 7.5 Hz, 2H, Ar), 7.97 (d, J = 17.0 Hz, 2H, CH═CH), 8.47−8.49 (m, 4H, Ar); ^{13}C NMR (75 MHz, $CDCl_3$, TMS, ppm) δ 156.73, 133.31, 132.92, 129.54,

TABLE 1: Crystal Data and Structure Refinements of Four Crystals

	DSA	BMOSA	B-4-BOSA	B-2-BOSA
empirical formula	$C_{30}H_{22}$	$C_{32}H_{26}O_2$	$C_{38}H_{38}O_2$	$C_{38}H_{38}O_2$
formula wt	382.48	442.53	526.68	526.68
T, K	293(2)	293(2)	293(2)	293(2)
crystal system	monoclinic	triclinic	triclinic	monoclinic
space group	$P2(1)/n$	$P\bar{1}$	$P\bar{1}$	$P2(1)/c$
a, Å	5.2500(10)	6.9598(14)	9.5989(19)	9.2404(18)
b, Å	9.4591(19)	8.8751(18)	12.563(3)	8.6917(17)
c, Å	20.734(4)	10.465(2)	14.354(3)	18.711(4)
α, deg	90	101.50(3)	110.05(3)	90
β, deg	90.70(3)	99.17(3)	107.52(3)	97.04(3)
γ, deg	90	105.19(3)	99.46(3)	90
V, Å^3	1029.6(4)	595.8(2)	1479.8(5)	1491.4(5)
Z	2	1	2	1
density, mg/m^3	1.234	1.233	1.182	0.586
μ (Mo Kα), mm^{-1}	0.070	0.075	0.071	0.035
θ range, deg	3.65−27.46	3.11−27.48	3.01−27.46	3.21−27.48
no. of reflcns collected	9805	5902	14445	14139
no. of unique reflcns	2348	2695	6619	3407
R(int)	0.0633	0.0496	0.0492	0.0436
GOF	1.074	1.020	1.006	1.108
R_1 [$I > 2\sigma(I)$]	0.0736	0.0620	0.0670	0.0882
wR_2 [$I > 2\sigma(I)$]	0.2221	0.1218	0.1571	0.2810
R_1 (all data)	0.1268	0.1400	0.1582	0.1293
wR_2 (all data)	0.2460	0.1477	0.1941	0.3171
final diff ρ_{max}, e·Å^{-3}	0.209, −0.252	0.148, −0.168	0.251, −0.279	0.501, −0.565

TABLE 2: Selected Dihedral Angles (deg) in Crystal Structures of 9,10-Distyrylanthracene Derivatives

compd	$\theta_{(1,2,3,4)}$	$\theta_{(2,3,4,5)}$	$\theta_{(3,4,5,6)}$	$\theta^*_{(3,4,5,6)}$
DSA	4.6	177.2	75.0	54.1
BMOSA	7.5	178.2	61.1	54.0
B-4-BOSA[a]	1.2	179.4	65.6	50.9
	7.1	177.3	71.8	
B-2-BOSA	21.5	176.0	64.6	52.4

[a] The crystal structure of B-4-BOSA is asymmetry, so there are two groups of selected dihedral angles in the crystal; $\theta^*_{(3,4,5,6)}$ corresponds to the selected dihedral angle $\theta_{(3,4,5,6)}$ in the molecular structures of 9,10-distyrylanthracene derivatives which were calculated by the DFT B3LYP/6-31G* level and performed with the Gaussian 03 package program.

128.89, 127.18, 126.63, 125.77, 125.00, 120.57, 111.93, 67.98, 31.39, 19.37, 13.82; MALDI/TOF MS calcd for $C_{38}H_{38}O_2$ 526.3, found 526.6. Anal. Calcd for $C_{38}H_{38}O_2$: C, 86.65; H, 7.27. Found: C, 86.54; H, 7.31.

Result and Discussion

Synthesis. Synthetic procedures for the four DSA derivatives are depicted in Scheme 1. All the compounds were obtained in all-trans conformations by Wittig condensation and trans-selective Heck coupling reaction, and were fully characterized by ^{1}H NMR, ^{13}C NMR, elemental analysis, and MALDI-TOF-MS.

Nonplanar Crystal Structures. Single crystals of 9,10-distyrylanthracene derivatives were prepared by vaporizing mixed solvents of chloroform and ethanol slowly at room temperature. Their crystal structures were determined by X-ray crystallography. Their crystal data and structure refinements are given in Table 1, and the selected dihedral angles are listed in Table 2. The crystal structures of the four DSA derivatives are shown in Chart 2. As we can see from Chart 1, for the four molecules, there are large torsions ($\theta_{(3,4,5,6)}$) between the anthracene center and vinylene moieties substituted at 9 and 10 positions because of the large internal steric hindrance. The torsional angles of the double bonds ($\theta_{(2,3,4,5)}$) are distributed from 176° to 179° which can be attributed to the effect of the π-electrons of the double bonds. The torsional angles ($\theta_{(1,2,3,4)}$) of DSA, BMOSA, and B-4-BOSA are less than 7.5°, while that of B-2-BOSA is a little bit larger (21.5°) due to the effect of internal steric hindrance between the vinylene moieties and the butoxy moieties. The analysis of the crystal structures of the four molecules demonstrates that they have a nonplanar conformation in their crystals. The change of the torsional angles indicates the effect of the intermolecular interactions and molecular stacking on the molecular conformations.

Supramolecular Interactions and Molecular Stacking Features. As shown in Chart 2, the backbones of the four molecules largely deviate from a plane and typical cofacial $\pi-\pi$ stacking becomes impossible. But from the analysis of the crystal structures, we found that the CH/π hydrogen bond[15] as a driving force plays a crucial role in the crystal packing and is also important in terms of the nonplanar conformations of the four compounds. As listed in Table 3, there are two CH/π hydrogen bonds in DSA, BMOSA, and B-2-BOSA, and four CH/π hydrogen bonds in B-4-BOSA. Two CH/π hydrogen bonds are formed between anthrylene (An) core and phenyl (Ph) rings, and another two CH/π hydrogen bonds are formed between butoxy (But) chains and phenyl rings in B-4-BOSA. Although B-2-BOSA has the same butoxy moieties with B-4-BOSA, there is no CH/π hydrogen bond formed between butoxy chains and other aromatic moieties, because of the disordered conformation of butoxy moieties of B-2-BOSA in the crystalline state.

The unit cell of DSA is monoclinic with space group $P2(1)/n$. As shown in Figure 1a, a CH/π hydrogen bond (interaction 1) is formed between two molecules with an interaction distance of 2.76 Å and an angle of 141.6°, where the vinylene (Vin) moiety along the long axis of one molecule acts as an H donor and the corresponding anthrylene core of the adjacent molecule acts as an H acceptor. At the same time, another CH/π hydrogen bond (interaction 2) is formed between two molecules with an interaction distance of 3.06 Å and an angle of 153.3°, where the phenyl ring acts as an H donor and the corresponding anthrylene core of the adjacent molecule acts as an H acceptor.

CHART 2: Molecular Structures of 9,10-Distyrylanthracene Derivatives

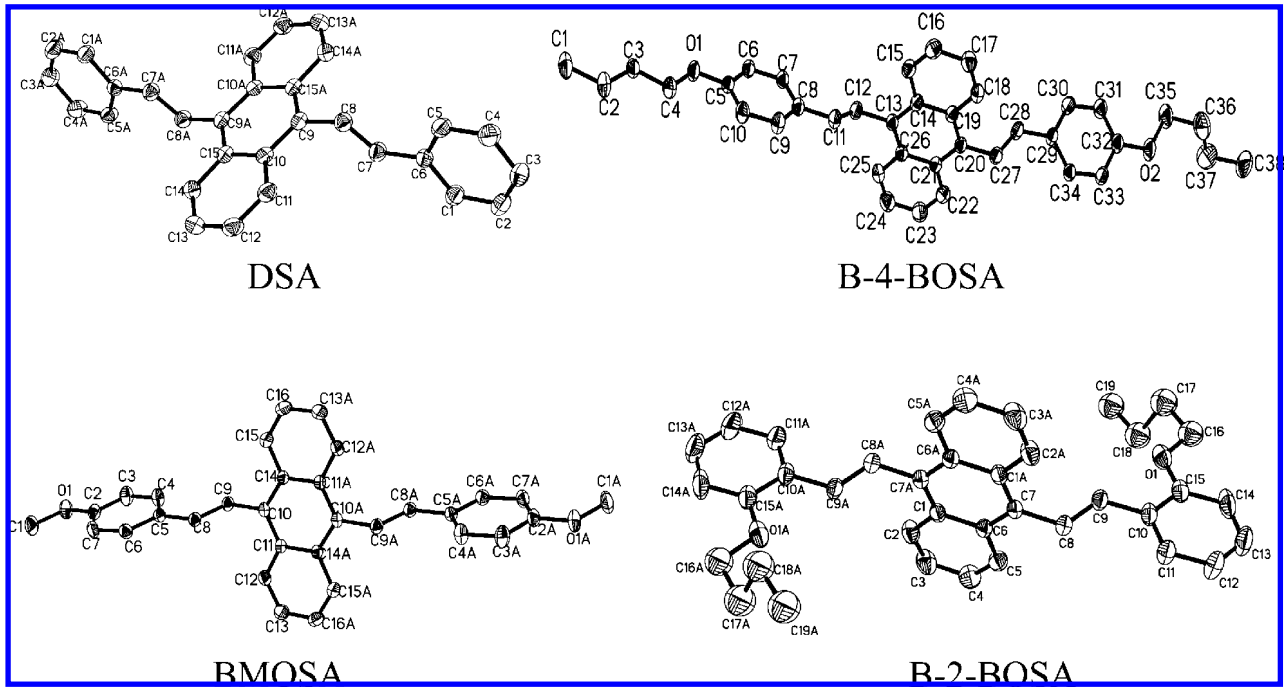

TABLE 3: Summary of the CH/π Interactions in Four Crystals

compound		orientation of interaction	distance of the H···ring (Å)	angle of the C−H···ring (deg)
DSA	**1**	Vin → An	2.76	141.6
	2	Ph → An	3.06	153.3
BMOSA	**3**	Ph → An	2.92	148.6
	4	An → Ph	2.92	144.0
B-4-BOSA	**5**	Ph → An	2.95	156.5
	6	An → Ph	3.12	131.4
	7	But → Ph	2.90	149.9
	8	But → Ph	2.80	173.3
B-2-BOSA	**9**	Ph → An	3.03	141.7
	10	An → Ph	3.26	147.1

Each DSA molecule connects with four adjacent molecules through six CH/π hydrogen bonds, and as a result, the intramolecular motions such as the twisting of the double bond and that of the end phenyl ring connected to the double bond are not free. Both of the strong supramolecular interactions not only make the molecule more rigid and stable in the crystal lattice, but also induce tight intermolecular packing. In the crystal of DSA, the molecules pack into molecular columns along the *a*-axis and slides to their neighbors along the long axis within one column due to interaction 1, as shown in Figure 1a. The distance (d_1) between two molecules within one column is measured to be 5.25 Å, which is too large to form the $\pi-\pi$ interaction. As shown in Figure 1b, the molecules are packing into "zigzag motif"[16] along a mirror glide plane in one layer due to interaction 2.

The unit cells of BMOSA and B-4-BOSA are triclinic with space group of $P\bar{1}$. As shown in Figures 2b and 3b, the two molecules pack into the simple "brickwall motif"[17] in which each "brick", or molecule, is situated over the gap between the bricks in the row below. The stacking arrangement of BMOSA is attributed to two CH/π hydrogen bonds between phenyl rings and the anthrylene core, as shown in Figure 2a (interactions 3 and 4). The interaction distance and the angle of the C−H−π center for interaction 3 are 2.92 Å and 148.6°, and those for interaction 4 are 2.92 Å and 144.0°, respectively. These two functional groups have the advantage of providing simultaneously H donor and H acceptor properties for CH/π hydrogen bonds. As for B-4-BOSA, the molecule in the crystal is asymmetric with different dihedral angles (Table 2, $\theta_{(1,2,3,4)}$, $\theta_{(2,3,4,5)}$, and $\theta_{(3,4,5,6)}$). The asymmetric molecule indicates the presence of considerable packing forces in the crystal stacking. Except for two CH/π hydrogen bonds formed between the phenyl ring and the anthrylene core (interaction 5 and 6), two more CH/π hydrogen bonds (interactions 7 and 8) are formed between the alkoxy chain and the adjacent phenyl ring (Figure 3a). The interaction distance and the angle of the C−H−π center for interaction 7 are 2.90 Å and 149.9°, and those for interaction 8 are 2.80 Å and 173.3°, respectively. The two CH/π hydrogen bonds with relatively short interaction distance may hinder the rotation of the terminal phenyl ring effectively.

B-2-BOSA crystallize in the monoclinic system with space group $P2(1)/c$. As shown in Figure 4b, the stacking image of B-2-BOSA is very similar to that of DSA except for the different intermolecular distance. The distance (d_2) between two adjacent molecules in B-2-BOSA is about 8.69 Å, which is much larger than that in DSA, because of steric hindrance induced by the large substituent at the 2 position of the phenyl ring. Although intermolecular distance becomes so large, there are also two CH/π hydrogen bonds that enable the molecules to accumulate tightly, as shown in Figure 4a (interactions 9 and 10). The interaction distance and the angle of the C−H−π center for interaction 9 are 3.03 Å and 141.7°, and those for interaction 10 are 3.26 Å and 147.1°, respectively. As in BMOSA, both of the interactions are formed between the phenyl ring and the anthracene ring in B-2-BOSA, and they act as H donors and H acceptors simultaneously.

The analysis of supramolecular interactions and molecular stacking features in the four compounds indicates that the supramolecular interactions considerably affect the degree of torsion and stacking feature of these molecules.

Aggregation-Induced Emission (AIE) Properties. Figure 5 outlines the absorption spectra of the four compounds in dilute tetrahydrofuran (THF) solutions. There are two main absorption

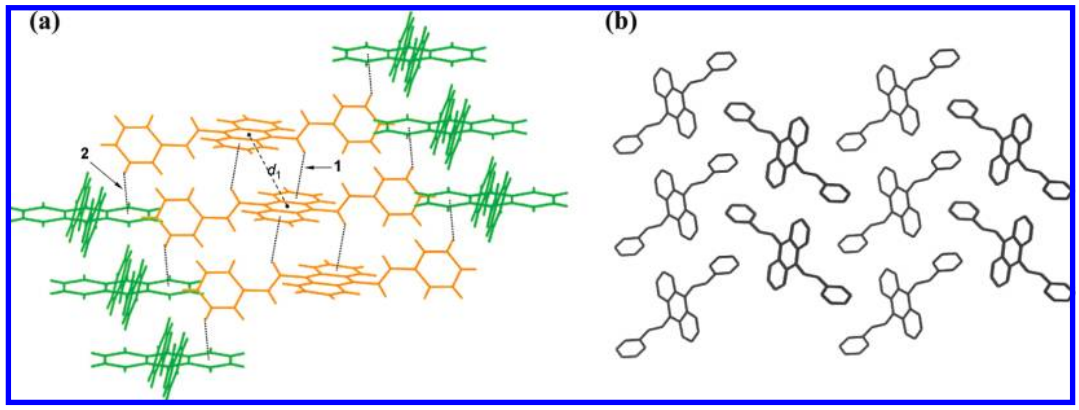

Figure 1. (a) The schematic intermolecular interactions of **1** and **2** in the crystal of DSA. The distance between two molecules within one column (d_1) is 5.25 Å. (b) Stacking images of DSA, viewed along the *a*-axis. The hydrogen atoms have been omitted for clarity.

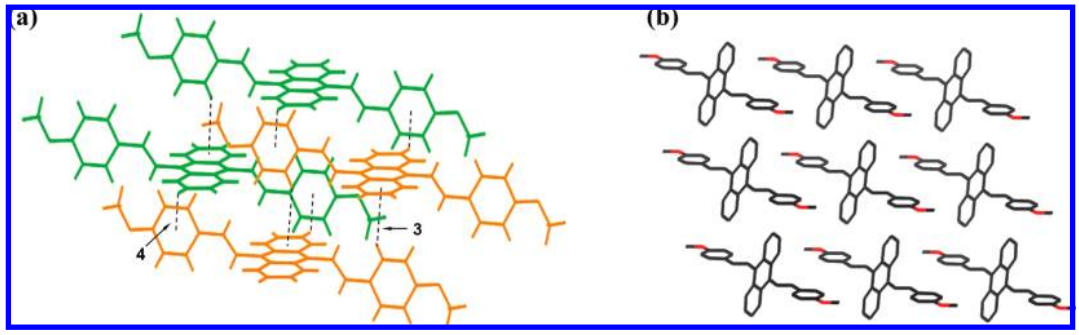

Figure 2. (a) The schematic intermolecular interactions of **3** and **4** in the crystal of BMOSA. (b) Stacking images of BMOSA, viewed along the *a*-axis. The hydrogen atoms have been omitted for clarity.

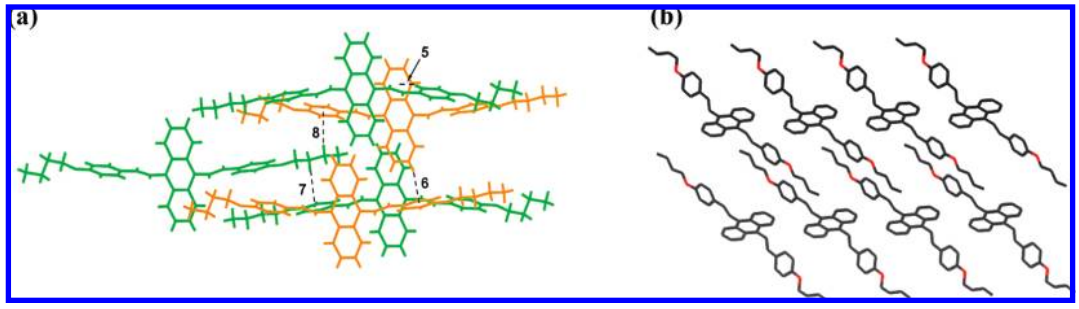

Figure 3. (a) The schematic intermolecular interactions of **5**, **6**, **7**, and **8** in the crystal of B-4-BOSA. (b) Stacking images of B-4-BOSA, viewed along the *b*-axis. The hydrogen atoms have been omitted for clarity.

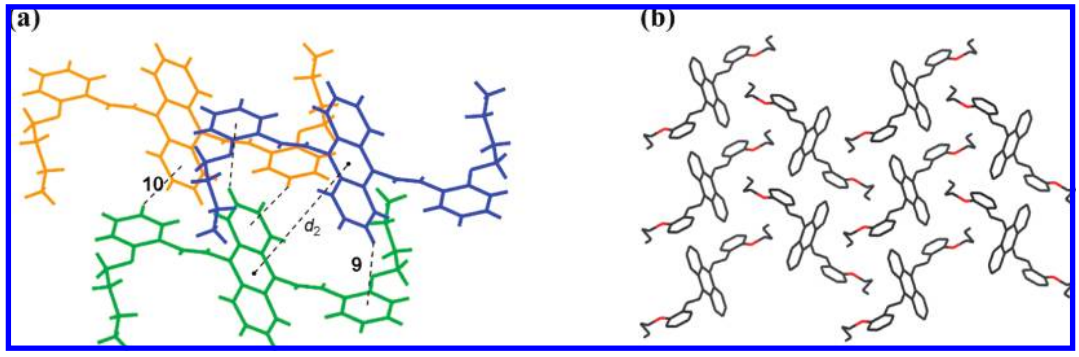

Figure 4. (a) The schematic intermolecular interactions of **9** and **10** in the crystal of B-2-BOSA. The distance between two molecules (d_2) is 8.69 Å. Molecular structure has been dealt with disorder treatment. (b) Stacking images of B-2-BOSA, viewed along the *a*-axis. The hydrogen atoms have been omitted for clarity.

bands in all four of the compounds: one located at about 307 nm corresponded to the absorption of the styryl segment, and the other located at about 414 nm is attributed to the $\pi-\pi^*$ transition. The formation of the nanoparticles in the mixture of good solvent (THF) and poor solvent (water) is easy to control by changing the ratios of the solvents. As shown in the absorption spectrum of the DSA derivatives in the THF/H_2O mixtures (Figure 6), their absorption bands are very similar to their absorption in dilute THF solutions, which is indicative of the absence of $\pi-\pi$ interaction in the nanoparticles due to the

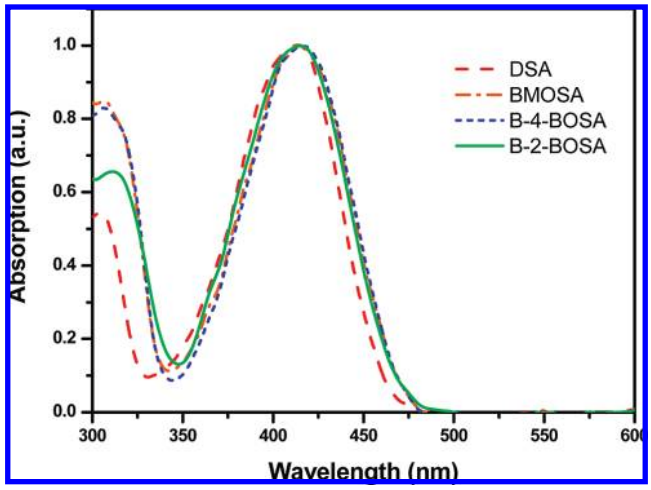

Figure 5. Normalized absorption spectra of the compounds in dilute THF solutions (10 μM).

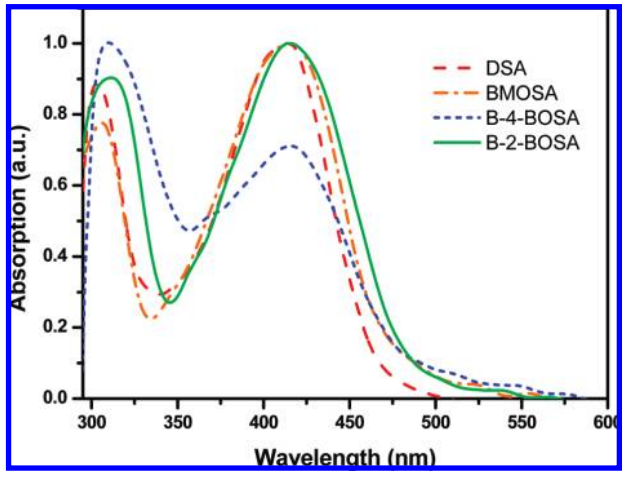

Figure 6. Normalized absorption spectra of the compounds in THF/H_2O mixture (THF/H_2O = 1:3 v/v).

large intermolecular distance. Also, level-off tails were obviously observed in the long-wavelength region of the absorption of the four compounds in the THF/H_2O mixtures. This was attributed to the Mie effect of the nanoparticles of the compounds.

The PL spectrum of the four compounds in dilute THF solutions is shown in Figure 7. All of the compounds exhibit weak, broad, and orange emission in molecularly dissolved solutions and the PL quantum efficiencies of the four compounds in dilute THF solutions are very low (Table 4), which means that the fluorescence of the compounds is quenched in solutions. The PL spectrum of the crystals of the four compounds is shown in Figure 8. They show intense, relatively narrow and green emission located around 520 nm with poor structure, except for that of B-2-BOSA, which is much more blue-shifted than the others. This large blue-shifted emission in the crystal of B-2-BOSA is due to the large distorted conformation of B-2-BOSA, as shown in Table 2 (see $\theta_{(1,2,3,4)}$). Compared with the crystalline state emissions of BMOSA and B-4-BOSA, the crystalline state emission of DSA is slightly blue-shifted. As we discussed above, DSA packs into the "zigzag motif" with relatively strong intermolecular CH/π interactions (given in Table 3), while BMOSA and B-4-BOSA pack into the "brick-wall motif" with relatively weak intermolecular CH/π interactions. It is the difference in the stacking mode and the difference

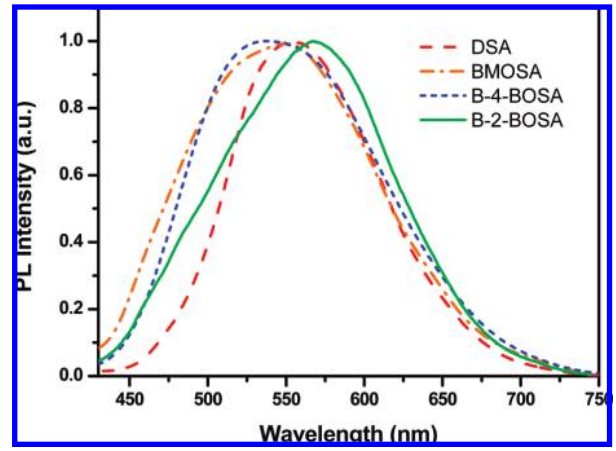

Figure 7. Normalized PL spectra of the compounds in dilute THF solutions (10 μM).

in the intermolecuar CH/π interactions that leads to different crystalline state emissions of the four compounds.

To gain insight into the AIE phenomenon of the DSA derivatives, the optimized conformations of a free monomer of the four compounds are calculated at the DFT B3LYP/6-31G* level and performed by the Gaussian 03 package program, respectively.[18] As shown in Table 2, the dihedral angle $\theta_{(3,4,5,6)}$ in the each crystal is larger than the dihedral angle $\theta^*_{(3,4,5,6)}$ optimized by DFT B3LYP/6-31G*. This larger dihedral angle is responsible for the blue-shift from crystal to solution. For example, the emission peak of DSA in crystal is located at 516 nm, while that in $CHCl_3$ solution is located at 556 nm. These intense, narrow, and blue-shifted emissions of the crystals compared to that of the solutions imply that the torsional motion is unambiguously restricted by steric interaction, leading to the closure of the nonradiative decay channel,[12a,19] and the more distorted conformations in their crystalline state limit effective conjugation, resulting in blue-shifted emissions of the crystals. The photophysical properties of the four compounds are listed in Table 4. As shown in Table 4, the PL efficiency of the four compounds in their crystalline state is from 18.7% to 50.8%, which is much higher than that in the dilute solution.

The AIE feature also can be characterized by the enhancement of the emission efficiency from the isolated molecules to the aggregate particles. For example, the PL spectrum of B-4-BOSA in a THF/H_2O mixture (with concentration being kept at 20 μM) is shown in Figure 8. A dramatic change of the fluorescence intensity of B-4-BOSA from the nonfluorescent THF solution to the strongly fluorescent suspension in 80% THF/H_2O mixture can be observed. The emission from the pure THF solution is so weak that its PL spectrum is virtually flat line parallel to the abscissa. In contrast, when large amounts of water are added into the solution, the PL of B-4-BOSA is switched on, with an intensity boost of about 100 times. Since water is a poor solvent of B-4-BOSA, the molecule has aggregated into solid particles in the THF/H_2O mixture with high water contents. The spectrum of the PL efficiency versus different THF/H_2O fractions is also shown in Figure 8. The PL efficiency in pure THF solution is less than 0.8%, and the isolated molecules show very weak fluorescence until 50% volume fractions of water were added. But at over 50% volume fractions of water added, the molecules aggregated into solid particles, and the PL efficiency increases dramatically with similar emission to that of the crystal.

Role of Restricted Intramolecular Torsion. Studies on the crystal structures and supramolecular interactions of single crystals can help us figure out the relationship between the

TABLE 4: Photophysical Properties of 9,10-Distyrylanthracene Derivatives

	abs (nm)		PL (nm)		$\Phi O_{PL\ (\%)}$	
material	solution	nanoparticle	solution	crystal	solution	crystal
DSA	304, 414	303, 414	555	516	0.4	50.8
BMOSA	307, 415	306, 415	550	523	0.7	40.5
B-4-BOSA	307, 417	309, 416	538	520	0.5	31.2
B-2-BOSA	313, 415	311, 415	567	501	2.3	18.7

molecular structure and the AIE property in this system. Compared to the classical aggregation-caused quenching od active molecule *trans*-distyrylbenzene,[20] the only difference in the molecular structure of DSA is that the anthrylene core substitutes the benzene core. As shown in Figure 9, the molecular structure of DSA (Figure 10) is significantly distorted at the attaching 9,10-positions of the anthrylene core because of the internal steric hindrance arising from the proximate hydrogens indicated by the dotted arrows. The distorted geometry makes the backbone deviate from a conjugated plane, which means that free intramolecular torsional motion in the solution can lead to fast nonradiative relaxation and reduce the PL quantum yield in the solution. In the crystalline state, however, the free torsional motion is obviously restricted by supramolecular interactions resulting in the closure of the nonradiative decay channel and enhanced fluorescence emission.

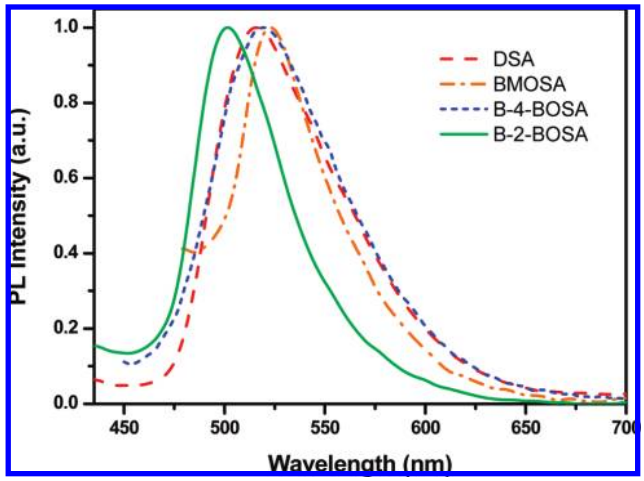

Figure 8. Normalized PL spectra of the compounds in the crystals.

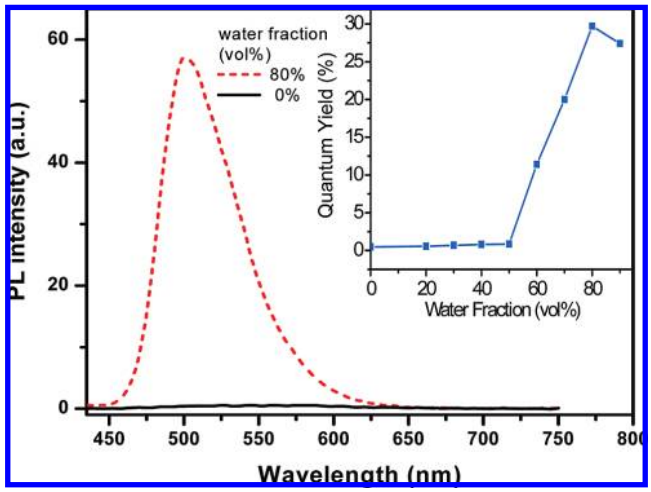

Figure 9. PL spectra of B-4-BOSA (20 μM) in the different THF/H_2O fraction solutions. The inset shows the change in the relative PL quantum yields of B-4-BOSA versus water fractions in THF (quinine sulfate was used as a standard).

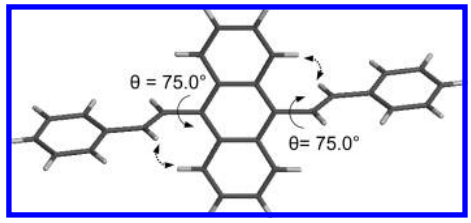

Figure 10. Molecular structure of DSA in crystal.

As discussed above, the restricted intramolecular torsion in DSA plays a crucial role in overcoming fluorescence quenching in the crystalline state and this large torsion angle in the crystal may be the reason for the high PL quantum efficiency. The other three compounds also have large restricted torsion angles in their crystals, which must be the key factor of crystallization-enhanced fluorescence. When we compare the four compounds, there are three commonalities: similar molecular structures, large restricted intramolecular torsion angles $\theta_{(3,4,5,6)}$, and enhanced fluorescence in the crystalline state, from which we can draw the conclusion that the AIE properties come from the DSA moieties in the backbones of all the compounds. Actually, the distorted conformations resulting from the internal steric hindrance between the anthrylene cores and vinylene moieties are the main origin of AIE properties.

Conclusion

In this study, we reported a class of DSA derivatives with AIE property. These four molecules have a nonplanar conformation in crystals, which is attributed to the CH/π hydrogen bonds leading to relatively tight packing and rigid molecules. They show weak, broad, and orange fluorescence in their solutions but intense, narrow, and green emission in their crystals. This AIE effect suggests that intramolecular torsional motions can act as efficient nonradiative pathways for the excited states to decay in solution and the suppression of torsional motions by the intermolecular interaction in the crystalline state leads to enhanced fluorescence. The investigation of the relationship between the crystal structures and AIE properties of the four DSA derivatives indicates that the DSA moiety is the key factor of the AIE property due to the restricted intramolecular torsion between the 9,10-anthylene core and the vinylene segment. This research work could be useful in understanding AIE properties of 9,10-distyrylanthracene derivatives and designing novel materials with high PL quantum efficiency.

Acknowledgment. This work was supported by the State Key Development Program for Basic Research of China (Grant No.2009CB623605), the National Natural Science Foundation of China (Grant No. 50673035), Program for New Century Excellent Talents in Universities of China Ministry of Education, the 111 Project (Grant No. B06009).

Supporting Information Available: Crystallographic information files (CIF) for the four compounds. This material is available free of charge via the Internet at http://pubs.acs.org.

References and Notes

(1) Tang, C. W.; VanSlyke, S. A. *Appl. Phys. Lett.* **1987**, *51*, 913.

(2) Friend, R. H.; Gymer, R. W.; Holmes, A. B.; Burroughes, J. H.; Marks, R. N.; Taliani, C.; Bradley, D. D. C.; Dos Santos, D. A.; Brédas, J. L.; Loğdlund, M.; Salaneck, W. R. *Nature* **1999**, *397*, 121.

(3) Bourroughes, J. H.; Bradley, D. D. C.; Brown, A. R.; Marks, R. N.; MacKay, K.; Friend, R. H.; Burn, P. L.; Homes, A. B. *Nature* **1990**, *347*, 539.

(4) Mitschke, U.; Bauerle, P. *J. Mater. Chem.* **2000**, *10*, 1471.

(5) Kasha, M.; Rawls, H. R.; Bayoumi, M. A. *Pure Appl. Chem.* **1965**, *11*, 371.

(6) Jenekhe, S. A.; Osaheni, J. A. *Science* **1994**, *265*, 765.

(7) Moffitt, M.; Farinha, J. P. S.; Winnik, M. A.; Rohr, U.; Müllen, K. *Macromolecules* **1999**, *32*, 4895.

(8) (a) Luo, J.; Xie, Z.; Lam, J. W. Y.; Cheng, L.; Chen, H.; Qiu, C.; Kwok, H. S.; Zhan, X.; Liu, Y.; Zhu, D.; Tang, B. Z. *Chem. Commun.* **2001**, 1740. (b) Xie, Z.; Yang, B.; Cheng, G.; Liu, L.; He, F.; Shen, F.; Ma, Y.; Liu, S. *Chem. Mater.* **2005**, *17*, 1287. (c) Yu, G.; Yin, S.; Liu, Y.; Chen, J.; Xu, X.; Sun, X.; Ma, D.; Zhan, X.; Peng, Q.; Shuai, Z.; Tang, B.; Zhu, D.; Fang, W.; Luo, Y. *J. Am. Chem. Soc.* **2005**, *127*, 6335. (d) Chen, J.; Xu, B.; Yang, K.; Cao, Y.; Sung, H. H.; Williams, I. D.; Tang, B. Z. *J. Phys. Chem. B* **2005**, *109*, 17086. (e) Tong, H.; Dong, Y.; Hong, Y.; Haussler, M.; Lam, J. W. Y.; Sung, H. H. Y.; Yu, X.; Sun, J.; Williams, I. D.; Kwok, H. S.; Tang, B. Z. *J. Phys. Chem. C* **2007**, *111*, 2287. (f) Dong, Y. Q.; Lam, J.-W. Y.; Qin, A. J.; Sun, J. X.; Liu, J. Z.; Li, Z.; Sun, J. Z.; Sung, H.-H. Y.; Williams, I. D.; Kwok, H. S.; Tang, B. Z. *Chem. Commun.* **2007**, 3255. (g) Tong, H.; Hong, Y.; Dong, Y.; Ren, Y.; Haussler, M.; Lam, J. W. Y.; Wong, K. S.; Tang, B. Z. *J. Phys. Chem. B* **2007**, *111*, 2000.

(9) (a) An, B. K.; Kwon, S. K.; Jung, S. D.; Park, S. Y. *J. Am. Chem. Soc.* **2002**, *124*, 14410. (b) Lim, S. J.; An, B. K.; Park, S. Y. *Macromolecules* **2005**, *38*, 6236. (c) Lim, S. J.; An, B. K.; Jung, S. D.; Chung, M. A.; Park, S. Y. *Angew. Chem., Int. Ed.* **2004**, *43*, 6346.

(10) (a) Funahashi, M.; Hanna, J. *Phys. Rev. Lett.* **1997**, *78*, 2184. (b) Schein, L. B.; McGhie, A. R. *Phys. Rev. B* **1979**, *20*, 1631.

(11) Though Schön et al. claimed that electrically pumped lasers were realized (Schön, J. H.; et al. *Science* **2000**, *289*, 599. *Science* **2000**, *290*, 963), the papers have since been retracted by the journal (*Science* **2002**, *298*, 961).

(12) (a) Kim, S.; Zheng, Q. D.; He, G. S.; Bharali, D. J.; Pudavar, H. E.; Baev, A.; Prasad, P. N. *Adv. Funct. Mater.* **2006**, *16*, 2317. (b) Kim, S.; Pudavar, H. E.; Bonoiu, A.; Prasad, P. N. *Adv. Mater.* **2007**, *19*, 3791. (c) Kim, S.; Ohulchanskyy, T. Y.; Pudavar, H. E.; Pandey, R. K.; Prasad, P. N. *J. Am. Chem. Soc.* **2007**, *129*, 2669.

(13) Nakatsuji, S.; Matsuda, K.; Uesugi, Y.; Nakashima, K.; Akiyama, S.; Katzer, G.; Fabian, W. *J. Chem. Soc., Perkin. Trans. 2* **1991**, 861.

(14) (a) Xia, H. J.; He, J. T.; Peng, P.; Zhou, Y. H.; Li, Y. W.; Tian, W. J. *Tetrahedron Lett.* **2007**, *48*, 5877. (b) Xia, H. J.; He, J. T.; Xu, B.; Wen, S. P.; Li, Y. W.; Tian, W. J. *Tetrahedron* **2008**, *64*, 5736.

(15) (a) Nishio, M. *CrystEngComm* **2004**, *6*, 130. (b) Xie, Z. Q.; Liu, L. L.; Yang, B.; Yang, G. D.; Ye, L.; Ma, Y. G. *Crst. Growth Des.* **2005**, *5*, 1959.

(16) Weiss, H. C.; Bläser, D.; Boese, R.; Doughan, B. M.; Haley, M. M. *Chem. Commun.* **1997**, 1703.

(17) Feast, W. J.; Lo̎venich, P. W.; Puschmann, H.; Taliani, C. *Chem. Commun.* **2001**, 505.

(18) Frisch, M. J.; Trucks, G. W.; Schlegel, H. B.; Scuseria, G. E.; Robb, M. A.; Cheeseman, J. R.; Montgomery, J. A., Jr.; Vreven, T.; Kudin, K. N.; Burant, J. C.; Millam, J. M.; Iyengar, S. S.; Tomasi, J.; Barone, V.; Mennucci, B.; Cossi, M.; Scalmani, G.; Rega, N.; Petersson, G. A.; Nakatsuji, H.; Hada, M.; Ehara, M.; Toyota, K.; Fukuda, R.; Hasegawa, J.; Ishida, M.; Nakajima, T.; Honda, Y.; Kitao, O.; Nakai, H.; Klene, M.; Li, X.; Knox, J. E.; Hratchian, H. P.; Cross, J. B.; Adamo, C.; Jaramillo, J.; Gomperts, R.; Stratmann, R. E.; Yazyev, O.; Austin, A. J.; Cammi, R.; Pomelli, C.; Ochterski, J. W.; Ayala, P. Y.; Morokuma, K.; Voth, G. A.; Salvador, P.; Dannenberg, J. J.; Zakrzewski, V. G.; Dapprich, S.; Daniels, A. D.; Strain, M. C.; Farkas, O.; Malick, D. K.; Rabuck, A. D.; Raghavachari, K.; Foresman, J. B.; Ortiz, J. V.; Cui, Q.; Baboul, A. G.; Clifford, S.; Cioslowski, J.; Stefanov, B. B.; Liu, G.; Liashenko, A.; Piskorz, P.; Komaromi, I.; Martin, R. L.; Fox, D. J.; Keith, T.; Al-Laham, M. A.; Peng, C. Y.; Nanayakkara, A.; Challacombe, M.; Gill, P. M. W.; Johnson, B.; Chen, W.; Wong, M. W.; Gonzalez, C.; Pople, J. A. *Gaussian 03*, Revision A.1; Gaussian, Inc., Pittsburgh, PA, 2003.

(19) (a) Valeur, B. *Molecular Fluorescence: Principles and Applications*; Wiley-VCH: Weinheim, Germany, 2001. (b) Rettig, W. *Angew. Chem., Int. Ed. Engl.* **1986**, *25*, 971.

(20) Colaneri, N. F.; Bradley, D. D. C.; Friend, R. H.; Burn, P. L.; Holmes, A. B.; Spangler, C. W. *Phys. Rev. B* **1990**, *42*, 11670.

JP900205K